

P-CNN: Pose-based CNN Features for Action Recognition

Guilhem Chéron*[†]

Ivan Laptev*
Inria

Cordelia Schmid[†]

firstname.lastname@inria.fr

Abstract

This work targets human action recognition in video. While recent methods typically represent actions by statistics of local video features, here we argue for the importance of structural information derived from human poses. To this end we propose a new Pose-based Convolutional Neural Network descriptor (P-CNN) for action recognition. The descriptor aggregates motion and appearance information along tracks of human body parts. We investigate different schemes of temporal aggregation and experiment with P-CNN features obtained both for automatically estimated and manually annotated human poses. We evaluate our method on the recent and challenging JHMDB and MPII Cooking datasets. For both datasets our method shows consistent improvement over the state of the art.

1. Introduction

Recognition of human actions is an important step toward fully automatic understanding of dynamic scenes. Despite significant progress in recent years, action recognition remains a difficult challenge. Common problems stem from the strong variations of people and scenes in motion and appearance. Other factors include subtle differences of fine-grained actions, for example when manipulating small objects or assessing the quality of sports actions.

The majority of recent methods recognize actions based on statistical representations of local motion descriptors [20, 29, 37]. Such an approach has been shown highly successful in recognizing coarse action (standing up, handshaking, dancing) in challenging scenes with camera motions, occlusions, multiple people, etc. This global approach, however, is lacking structure and may not be optimal to recognize subtle variations, e.g. to distinguish correct and incorrect golf swings or to recognize fine-grained cooking actions illustrated in Figure 5.

*WILLOW project-team, Département d'Informatique de l'École Normale Supérieure, ENS/Inria/CNRS UMR 8548, Paris, France.

[†]LEAR project-team, Inria Grenoble Rhône-Alpes, Laboratoire Jean Kuntzmann, CNRS, Univ. Grenoble Alpes, France.

Fine-grained recognition in static images highlights the importance of spatial structure and spatial alignment as a pre-processing step. Examples include alignment of faces for face recognition [2] as well as alignment of body parts for recognizing species of birds [12]. Drawing analogy to this prior work, we believe action recognition will benefit from the spatial and temporal structure of human poses.

In this work we design a new action descriptor based on human poses. Provided with tracks of body joints over time, our descriptor combines motion and appearance features for body parts. Given the recent success of Convolutional Neural Networks (CNN) [21, 18], we explore CNN features obtained separately for each body part in each frame. We use appearance and motion-based CNN features computed for each track of body parts, and investigate different schemes of temporal aggregation. The pipeline for our *Pose-based Convolutional Neural Network* (P-CNN) features is illustrated in Figure 1.

Pose estimation in natural images is still a difficult task [6, 33, 38]. In this paper we investigate P-CNN features both for automatically estimated and manually annotated human poses. We experiment on two challenging datasets: JHMDB [17], a subset of HMDB [19] for which manual annotation of human poses have been provided by [17], as well as MPII Cooking Activities [26], composed of a set of fine-grained cooking actions. Evaluation of our method on both datasets consistently outperforms the human pose-based descriptor HLPF [17]. Combination of our method with Dense trajectory features [37] improves state of the art for both datasets. The code for our P-CNN method will be publicly available upon publication.

The rest of the paper is organized as follows. Related work is discussed in Section 2. Section 3 introduces our P-CNN feature. We summarize state-of-the-art methods in Section 4 and present datasets in Section 5. Section 6 evaluates our method and compares it to the state of the art. Section 7 concludes the paper.

2. Related work

Action recognition in the last decade has been dominated by local features [20, 29, 37]. In particular, Dense

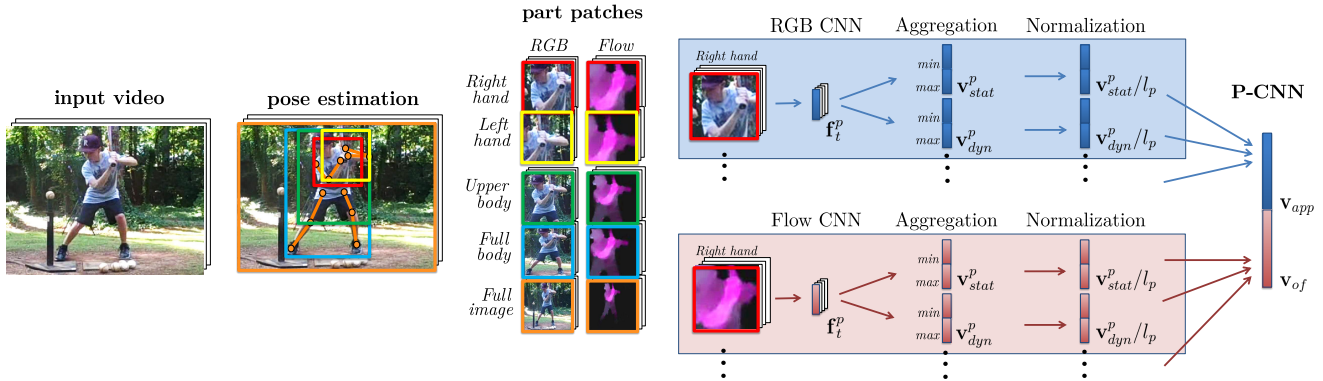


Figure 1: P-CNN construction pipeline. From left to right: Input video. Human pose and our human body parts for one frame of the video. Part appearance (RGB) and flow patches for our human body parts. One RGB and one flow CNN descriptor f_t^p is extracted per frame t and per part p (example is shown for the human body part *right hand*). Static frame descriptors f_t^p (resp. frame descriptor differences of f_t^p) are aggregated (using *min* and *max*) to obtain the video descriptor v_{stat}^p (resp. v_{dyn}^p). Video descriptors are normalized and concatenated over parts p and aggregation schemes into v_{app} and v_{of} . Our final P-CNN feature is the concatenation of RGB and flow features.

Trajectory (DT) features [37] combined with Fisher Vector (FV) aggregation [24] has recently shown outstanding results for a number of challenging benchmarks. We use DT-FV [37] as a strong baseline and experimentally demonstrate its complementarity to our method.

Recent advances in Convolutional Neural Networks (CNN) [21] have resulted in significant progress in image classification [18] and other vision tasks [15, 34, 32]. In particular, the transfer of pre-trained network parameters to problems with limited training data has shown success e.g. in [15, 23, 30]. Application of CNNs to action recognition in video, however, has shown only limited improvements so far [30, 39]. We extend previous global CNN methods and address action recognition using CNN descriptors at the local level of human body parts.

Most of the recent methods for action recognition deploy global aggregation of local video descriptors. Such representations provide invariance to numerous variations in the video but may fail to capture important spatio-temporal structure. Alternative methods represent actions using positions and temporal evolution of body joints. While reliable human pose estimation is still a challenging task, the recent study [17] reports significant gains provided by dynamic human pose features in cases when reliable pose estimation is available. We extend the work [17] and design a new CNN-based representation for human actions combining positions, appearance and motion of human body parts.

Our work builds on methods for human pose estimation in images [27, 25, 34, 38] and video sequences [7, 28]. In particular, we build on the method [7] and extract temporally-consistent tracks of body joints from video sequences. While our pose estimator is imperfect, we use

it to derive CNN-based pose features providing significant improvements for action recognition for two challenging datasets.

3. P-CNN: Pose-based CNN features

We believe human pose is essential for action recognition. Here we use positions of body joints to define informative image regions. We further borrow inspiration from [30] and represent body regions with motion-based and appearance-based CNN descriptors. Such descriptors are extracted at each frame and then aggregated over time to form a video descriptor. The pipeline for constructing P-CNN features is illustrated in Figure 1 and its details are explained below.

To construct P-CNN features, we first compute optical flow using [3] for each consecutive pair of frames. Following [16], the values of the motion field v_x, v_y are transformed to the $[0, 255]$ interval as $\tilde{v}_{x|y} = av_{x|y} + b$ with $a = 16$ and $b = 128$. The values below 0 and above 255 are truncated. We save transformed flow maps as images with three channels corresponding to motion \tilde{v}_x, \tilde{v}_y and the flow magnitude.

Given a video frame and corresponding positions of body joints, we crop RGB image patches and flow patches for *right hand*, *left hand*, *upper body*, *full body* and *full image* as illustrated in Figure 1. Each patch is resized to 224×224 pixels to match CNN input layer. To represent appearance and motion patches, we use two distinct CNNs with similar architecture to [18]. Both networks contain 5 convolutional and 3 fully-connected layers. The output of the second fully-connected layer with $k = 4096$ values is used for P-CNN descriptor. For RGB patches we use

the publicly available ‘‘VGG-f’’ network from [5] that has been pre-trained on the ImageNet ILSVRC-2012 challenge dataset [10]. For flow patches, we use the motion network provided by [16] that has been pre-trained for action recognition task on the UCF101 dataset [31].

Given descriptors \mathbf{f}_t^p for each part p and each frame t of the video, we next proceed with the aggregation of \mathbf{f}_t^p over all frames to obtain a fixed-length video descriptor. We consider *min* and *max* aggregations by computing minimum and maximum values for each descriptor dimension i over T video frames

$$\begin{aligned} m_i &= \min_{1 \leq t \leq T} \mathbf{f}_t^p(i), \\ M_i &= \max_{1 \leq t \leq T} \mathbf{f}_t^p(i). \end{aligned} \quad (1)$$

The *static video descriptor* for part p is defined by the concatenation of time-aggregated frame descriptors as

$$\mathbf{v}_{stat}^p = [m_1, \dots, m_k, M_1, \dots, M_k]^\top. \quad (2)$$

To capture temporal evolution of per-frame descriptors, we also consider temporal differences of the form $\Delta \mathbf{f}_t^p = \mathbf{f}_{t+\Delta t}^p - \mathbf{f}_t^p$ for $\Delta t = 4$ frames. Similar to (1) we compute minimum Δm_i and maximum ΔM_i aggregations of $\Delta \mathbf{f}_t^p$ and concatenate them into the *dynamic video descriptor*

$$\mathbf{v}_{dyn}^p = [\Delta m_1, \dots, \Delta m_k, \Delta M_1, \dots, \Delta M_k]^\top. \quad (3)$$

Finally, video descriptors for motion and appearance for all parts and different aggregation schemes are normalized and concatenated into the P-CNN feature vector. The normalization is performed by dividing video descriptors by their corresponding l_p (average L_2 -norm of the \mathbf{f}_t^p from the training set).

In Section 6 we evaluate the effect of different aggregation schemes as well as the contributions of motion and appearance features for action recognition. In particular, we compare ‘‘Max’’ vs. ‘‘Max/Min’’ aggregation where ‘‘Max’’ corresponds to the use of M_i values only while ‘‘Max/Min’’ stands for the concatenation of M_i and m_i defined in (2) and (3). We also try P-CNN features with and without dynamic descriptors where the concatenation of static and dynamic descriptors will be denoted by ‘‘Dyn’’. P-CNN training is performed using a linear SVM.

4. State-of-the-art methods

In this section we present the state-of-the-art methods used and compared to in our experiments. We first present the approach for human pose estimation in videos [7] used in our experiments. We then present state-of-the-art high-level pose features (HLPF) [17] and improved dense trajectories [37].

4.1. Pose estimation

To compute P-CNN features as well as HLPF features, we need to extract human pose from videos. We have implemented a video pose estimator based on [7]. We first extract poses for individual frames using the state-of-the-art approach of Yang and Ramanan [38]. Their approach is based on a deformable part model to locate positions of body joints (head, elbow, wrist...). We re-train their model on the FLIC dataset [27].

Following [7], we extract a large set of pose configurations in each frame and link them throughout the video using Dynamic Programming (DP). The poses selected with DP are constrained to have a high score of the pose estimator [38]. At the same time, the motion of joints in a pose sequence is constrained to be consistent with the optical flow extracted at joint positions. Differently to [7] we do not perform *limb recombination*. Some correctly estimated poses and failure cases are illustrated in Figure 2.

4.2. High-level pose features (HLPF)

High-level pose features (HLPF) compute spatial and dynamic relations between body joint positions and were introduced by [17]. Given a sequence of human poses P for a video clip, joint positions are first normalized with respect to the human scale. Then, their relative positions to the head are computed for each pose in P . We have observed that the head is more reliable than the torso used in [17]. Features are, then, the distances between all pairs of joints, orientations of the vectors connecting pairs of joints and inner angles spanned by vectors connecting all triplets of joints. These are the static features.

Dynamic features are obtained by cutting P into trajectories, in which differences (in time) of some of the static feature types are considered: differences between the distances between all pairs of joints, the orientations of the vectors connecting two joints and the inner angles. Furthermore, translations of joint positions (dx and dy) and their orientations ($\arctan(\frac{dy}{dx})$) are added.

To quantize the features, a codebook is computed for each descriptor type using k -means with $k = 20$. A video sequence is then described by a histogram and training is performed using an SVM with a χ^2 kernel. More details can be found in [17]. To compute HLPF features we re-use the publicly available code with slight modifications. As mentioned previously, we consider the head instead of the torso center for relative positions. We have also found that converting angles, originally in degrees, to radians and L_2 normalizing the HLPF features improve their performance.

4.3. Dense trajectory features

Dense Trajectories [35] are local video descriptors that have recently shown excellent performance in several action recognition benchmarks [22, 36]. The method first



Figure 2: Illustration of human pose estimation used in our experiments [7]. Successful examples and failure cases on JHMDB (left two images) and on MPII Cooking Activities (right two images). Only left and right arms are displayed for clarity.

densely samples points which are tracked using optical flow [13]. For each trajectory, 4 descriptors are computed in the aligned spatio-temporal volume: HOG [8], HOF [20] and MBH [9]. A recent approach [37] removes trajectories consistent with the camera motion (estimated computing a homography using optical flow and SURF [1] point matches and RANSAC [14]). Flow descriptors are then computed from optical flow warped according to the estimated homography. In our experiments we use this improved version of DT and rely on the online available code of [37].

Fisher Vectors (FV) [24] encoding has demonstrated classification results improvement over the bag-of-words approach in general [4] and their use with DT has been introduced in [22]. FV relies on a Gaussian mixture model (GMM) with K Gaussian components, computing first and second order statistics with respect to the GMM. FV encoding is performed separately for 4 different DT descriptors (their dimensionality is divided by a factor of 2 after PCA reduction). Following [24], the performance is improved by passing FV through signed square-rooting and L_2 normalization. As in [22] we use a spatial pyramid representation and a number of $K = 256$ Gaussian components. FV encoding is performed using the Yael library [11] while DT-FV training is done using a linear SVM.

5. Datasets

In our experiments we use two datasets JHMDB [17] and MPII Cooking Activities [26], as well as two subsets of these datasets sub-JHMDB and sub-MPII Cooking. We present them in the following.

JHMDB [17] is a subset of HMDB [19], see Figure 2 (left). It contains 21 human actions, such as *brush hair*, *climb*, *golf*, *run* or *sit*. Video clips are restricted to the duration of the action. There are between 36 and 55 clips per action for a total of 928 clips. Each clip contains between 15 and 40 frames of size 320×240 . Human pose is annotated in each of the 31838 frames. There are 3 train/test splits for the JHMDB dataset and evaluation averages the results over these three splits. The metric used is accuracy: each clip

is assigned an action label corresponding to the maximum value among the scores returned by the action classifiers.

In our experiments we also use a subset of JHMDB, referred to as **sub-JHMDB**[17]. This subset includes 316 clips distributed over 12 actions in which the human body is fully visible. Again there is a 3 train/test splits and the evaluation metric is accuracy.

MPII Cooking Activities [26] contains 64 fine grained actions and an additional background class, see Figure 2 (right). Actions take place in a kitchen with static background. There are 5609 action clips of frame size 1624×1224 . Some actions look very similar like *cut dice*, *cut slices*, and *cut stripes* or *wash hands* and *wash objects*, which is why activities are qualified as “fine grained”. There are 7 train/test splits and evaluation is reported, using the code provided with the dataset, in terms of mean Average Precision (mAP).

We have also defined a subset, referred to by **sub-MPII cooking**, which includes the classes *wash hands* or *wash objects*. We have selected these two classes as they are visually similar and differ mainly in the “object” manipulated. In order to analyze in detail the performance for these two classes we annotated human pose (body joints) in all frames. There are 55 and 139 clips respectively for *wash hands* and *wash objects* actions, for a total of 29,997 frames.

6. Experimental results

This section describes our experimental results and examines the effect of different design choices. First, we evaluate the complementarity of different human parts in Section 6.1. We then compare different variants for aggregating CNN features in Section 6.2. Next, we analyze the robustness of our features to errors in the pose and their ability to classify fine grained actions in Section 6.3. Finally, we compare our features to the state of the art and show that they are complementary to the popular dense trajectory features in Section 6.4.

6.1. Performance of human part features

Table 1 compares the performance of human part CNN features for both appearance and flow on JHMDB-GT (the JHMDB dataset with ground-truth pose) and MPII Cooking-Pose [7] (the MPII Cooking dataset with pose estimated by [7]). Note that we do not detect the full body for MPII Cooking, as in most frames only the upper body is visible.

Conclusions for both datasets are similar. We can observe that all human parts (hands, upper body, full body) as well as the full image have similar performance and that their combination improves the performance significantly. Removing one part at a time from this combination always results in a drop in performance (results not shown here). We, therefore, conclude that all pose parts together with the full image descriptor should be used jointly. We can also observe that flow descriptors consistently outperform appearance descriptors by a significant margin for all parts as well as the overall combination *All*. Furthermore, we can observe that the combination of appearance and flow further improves the performance for all parts including their combination *All*. This is the pose representation used in the following.

6.2. Aggregating P-CNN features

In the previous section we have applied a max-aggregation (see Section 3) for aggregating per-frame features into a video descriptor. We next compare alternative aggregation schemes.

As a first step, CNN features f_t are extracted for each frame, see Figure 1. Aggregation pools feature values for each dimension over all frames of the video. Results for max-aggregation on JHMDB-GT are reported in Table 1 and also in the first row of Table 2 for comparison. The following rows of Table 2 show the impact of adding min-aggregation (*Max/Min-aggr*) and first-order difference between CNN features (*All-Dyn*). Extracting single CNN features and their first-order differences combined with max- and min-aggregation (*All-Dyn (Max/Min-aggr)*) further improves the results. Overall, we obtain the best results with *All-Dyn(Max/Min-aggr)*, i.e., an accuracy improvement of 2.1%, 1.1% and 1.2% for App, OF and App+OF.

As explained in Section 3, the CNN variant corresponding to the final version of our P-CNN is *App+OF* with *All-Dyn(Max/Min-aggr)* (last column, last row) obtaining 74.6% accuracy on JHMDB-GT. On MPII Cooking-Pose [7] this final version of P-CNN achieves 62.3% mAP (as reported in Table 4) leading to an 1.5% improvement over max-aggregation reported in Table 1.

We also experimented with second-order differences and other statistics, such as mean-aggregation, but this did not improve our results. Furthermore, we implemented a score aggregation over classification scores obtained for individ-

| Aggregation scheme | App | OF | App+OF |
|------------------------|-------------|-------------|-------------|
| All (Max-aggr) | 60.4 | 69.1 | 73.4 |
| All (Max/Min-aggr) | 60.6 | 68.9 | 73.1 |
| All-Dyn (Max-aggr) | 62.4 | 70.6 | 74.1 |
| All-Dyn (Max/Min-aggr) | 62.5 | 70.2 | 74.6 |

Table 2: Comparison of different aggregation schemes: *Max*- and *Max/Min*-aggregations as well as adding first-order differences (*Dyn*). Results are given for appearance (*App*), optical flow (*OF*) and App + OF on JHMDB-GT (accuracy).

ual frames. This led to a decrease of performance, e.g. for *All (App)* on JHMDB-GT score-max-aggregation results in 56.1% accuracy, compared to 60.4% for features-max-aggregation (top row, left column in Table 2). This indicates that early aggregation works significantly better.

In the following we will report results for our final version of P-CNN, i.e., *All parts App+OF* with *Dyn(Max/Min-aggr)*.

6.3. Robustness of pose-based features

This section examines the robustness of our P-CNN features in the presence of errors in the pose estimation and compares to state-of-the-art pose features HLPF [17]. We report results obtained with the online available code modified as described in Section 4.2. Results are comparable in general and slightly better on JHMDB-GT (77.8% versus 76.0% reported in [17]). Table 3 evaluates the impact of automatic pose estimation versus ground-truth pose (GT) for sub-JHMDB and JHMDB. We can observe that results for GT pose are comparable on both datasets and for both type of pose features. However, P-CNN are significantly more robust to errors in pose estimation. If the pose is estimated automatically with state-of-the-art algorithms P-CNN drops by 5.7% on sub-JHMDB and 13.5% on JHMDB whereas HLPF drops by 13.5% and 52.5%. For both descriptors the drop is less significant on sub-JHMDB, as this subset only contains full human poses for which pose is easier to estimate. Overall the performance of P-CNN features for automatically extracted pose is excellent and outperforms HLPF by a very large margin (+36.1%) on JHMDB.

We now evaluate the robustness and compare to HLPF on the MPII cooking dataset. To evaluate the impact of ground-truth pose (GT) we have manually annotated two classes “washing hand” and “washing objects”, referred to by sub-MPII Cooking. Table 4 compares P-CNN and HLPF for sub-MPII and MPII Cooking. In all cases P-CNN outperforms HLPF significantly. Interestingly, even for ground-truth poses P-CNN performs significantly better than HLPF. This can be explained by the characteristics of “washing hands” and “washing objects”, which differ in the action object better described by our P-CNN, in particular

| Parts | JHMDB-GT | | | MPII Cooking-Pose [7] | | |
|------------|-------------|-------------|-------------|-----------------------|-------------|-------------|
| | App | OF | App + OF | App | OF | App + OF |
| Hands | 46.3 | 54.9 | 57.9 | 39.9 | 46.9 | 51.9 |
| Upper body | 52.8 | 60.9 | 67.1 | 32.3 | 47.6 | 50.1 |
| Full body | 52.2 | 61.6 | 66.1 | - | - | - |
| Full image | 43.3 | 55.7 | 61.0 | 28.8 | 56.2 | 56.5 |
| All | 60.4 | 69.1 | 73.4 | 43.6 | 57.4 | 60.8 |

Table 1: Performance of human part CNN features for appearance (App) and flow (OF). Results are obtained with max-aggregation on JHMDB-GT (accuracy) and MPII Cooking Activities-Pose [7] (mAP).

| sub-JHMDB | | | |
|-----------|------|-----------|------|
| | GT | Pose [38] | Diff |
| P-CNN | 72.5 | 66.8 | 5.7 |
| HLPF | 78.2 | 51.1 | 27.1 |

| JHMDB | | | |
|-------|------|----------|------|
| | GT | Pose [7] | Diff |
| P-CNN | 74.6 | 61.1 | 13.5 |
| HLPF | 77.8 | 25.3 | 52.5 |

Table 3: Impact of automatic pose estimation versus ground-truth pose (GT) for P-CNN features and HLPF [17]. Results are presented for sub-JHMDB and JHMDB (accuracy).

| sub-MPII Cooking | | | |
|------------------|------|----------|------|
| | GT | Pose [7] | Diff |
| P-CNN | 83.6 | 67.5 | 16.1 |
| HLPF | 76.2 | 57.4 | 18.8 |

| MPII Cooking | |
|--------------|----------|
| | Pose [7] |
| P-CNN | 62.3 |
| HLPF | 32.6 |

Table 4: Impact of automatic pose estimation versus ground-truth pose (GT) for P-CNN features and HLPF [17]. Results are presented for sub-MPII Cooking and MPII Cooking (mAP).

the hand feature. We can also observe that the drop due to pose estimation is similar for P-CNN and HLPF. This might be explained by the fact that CNN hands features are quite sensitive to the pose estimation. However, P-CNN still significantly outperforms HLPF for automatic pose. In particular, there is a significant gain of +29.7% for the full MPII Cooking dataset.

| Method | JHMDB | | MPII Cook. |
|---------------|-------------|-------------|-------------|
| | GT | Pose [7] | Pose [7] |
| P-CNN | 74.6 | 61.1 | 62.3 |
| DT-FV | 65.9 | 65.9 | 67.6 |
| P-CNN + DT-FV | 79.5 | 72.2 | 71.4 |

Table 5: Comparison to DT-FV on JHMDB (accuracy) and MPII Cooking Activities (mAP) for ground-truth (GT) and pose [7]. The combination of P-CNN + DT-FV performs best.

6.4. Comparison to the state of the art

In this section we compare to state-of-the-art dense trajectory features [37] encoded by Fisher vectors [22] (DT-FV), briefly described in Section 4.3. We use online available code, which we validated on Hollywood2 (65.3% versus 64.3% [37]). Furthermore, we show that our pose features P-CNN and DT-FV are complementary and compare to other state-of-the-art approaches on JHMDB and MPII Cooking.

Table 5 shows that for ground-truth poses our P-CNN features outperform state-of-the-art DT-FV descriptors significantly (8.7%). If the pose is extracted automatically both methods are on par. Furthermore, in all cases the combination of P-CNN and DT-FV obtained by late fusion of the individual classification scores significantly increases the performance over using individual features only. Figure 4 illustrates per-class results for P-CNN and DT-FV on JHMDB-GT.

Table 6 compares our results to state-of-the-art results on MPII Cooking. Our approach outperforms the state-of-the-art on this dataset. On JHMDB [17] we have compared to the state of the art [17] in the previous section. We perform on par for GT poses and significantly better for automatic poses. Combining our P-CNN with DT-FV further improves the performance to 79.5% for GT and to 72.2% for estimated pose [7], see Table 5. This improves over the state of the art [17].

Qualitative results comparing P-CNN and DT-FV are illustrated in Figure 3. A quantitative comparison is shown



Figure 3: Results on JHMDB-GT (split 1). Each column corresponds to an action. Examples on the left (green) show the 2 examples per action with the most significant improvement in ranking between P-CNN (rank in green) and DT-FV (rank in red). The examples on the right (red) show, similarly, the 2 largest decreases in ranking. Actions with large differences in performance are selected according to Figure 4. For each video sample, the middle frame is presented.

| Method | MPII Cook. |
|------------------------|------------|
| Holistic + Pose [26] | 57.9 |
| Semantic Features [40] | 70.5 |
| P-CNN + DT-FV (our) | 71.4 |

Table 6: State of the art on the MPII Cooking (mAP).

in Figure 4. To highlight improvements achieved by our P-CNN descriptor, we show results for classes with a large improvement of P-CNN over DT-FV, as such as *shoot_gun*, *wave*, *throw* and *jump* as well as for a class with a significant drop, namely *kick_ball*. Figure 3 shows two examples for each of the selected actions with the maximum difference in ranks obtained by P-CNN (green) and DT-FV (red). As an example the most significant improvement (Figure 3, top left) increases the sample ranking from 211 to 23, when replacing DT-FV by P-CNN. In particular, the *shoot_gun* and *wave* classes involve small localized motion, making classification difficult for DT-FV while P-CNN benefits from the local human body part information. Similarly, the two samples from the action class *throw* also seem to have restricted and localized motion while the action *jump* is very short in time. In the case of *kick_ball* the significant decrease can be explained by the important dynamics of this action, which is better captured by DT-FV features. Note that our P-CNN only captures motion information between two consecutive frames.

Figure 5 presents qualitative results for MPII Cooking-Pose [7] showing samples with the maximum difference in ranks over all classes.

7. Conclusion

This paper introduces a pose-based convolutional neural network feature (P-CNN). Appearance and flow information is extracted at decisive positions obtained from human

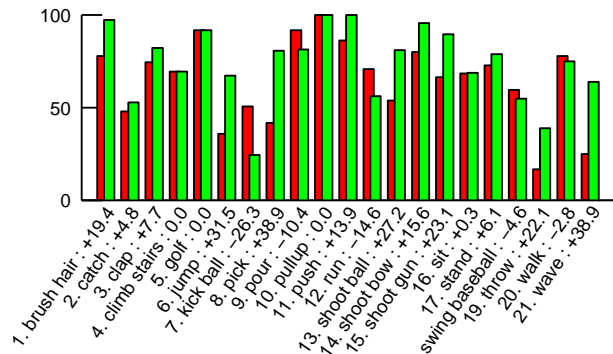


Figure 4: Per class accuracy on JHMDB-GT for P-CNN (green) and DT-FV (red). Numbers correspond to the accuracy difference between P-CNN and DT-FV (positive indicates that P-CNN performs better).

pose and aggregated over frames of a video. Our P-CNN description is shown to be significantly more robust to imprecise state-of-the-art human pose estimation than existing pose features based on joint relations [17]. P-CNN also significantly outperforms them when actions to differentiate are very similar as is the case for fine-grained actions of MPII Cooking Activities. More generally, P-CNN features are complementary to dense trajectories features and significantly improve the current state of the art on action recognition when combined with them.

Our study confirms the results of [17] that, when body joints are annotated, pose-based features consistently outperform state-of-the-art methods. This means that pose is crucial to capture discriminative information of human actions. Pose-based action recognition methods have a promising future due to recent large progress in pose estimation, notably using CNN [6]. Also, an interesting di-



Figure 5: Results on MPII Cooking-Pose [7] (split 1). Examples on the left (green) show the 8 best ranking improvements (over all classes) obtained by using P-CNN (rank in green) instead of DT-FV (rank in red). The examples on the right (red) show, similarly, the 2 largest decreases in ranking. For each video sample, the middle frame is presented.

rection for future work could be to adapt CNNs for each P-CNN part (hands, upper body, ...) by fine-tuning them for their specific area. This should further improve their performance.

Acknowledgements

This work was supported by the MSR-Inria joint lab, a Google Research Award, the ERC grant Activia and the ERC advanced grant ALLEGRO.

References

- [1] H. Bay, A. Ess, T. Tuytelaars, and L. Van Gool. Speeded-up robust features (surf). *Comput. Vis. Image Underst.*, pages 346–359, 2008. 4
- [2] T. Berg and P. N. Belhumeur. Poof: Part-based one-vs.-one features for fine-grained categorization, face verification, and attribute estimation. In *CVPR*, pages 955–962, 2013. 1
- [3] T. Brox, A. Bruhn, N. Papenberger, and J. Weickert. High accuracy optical flow estimation based on a theory for warping. In *ECCV*, pages 25–36. 2004. 2
- [4] K. Chatfield, V. Lempitsky, A. Vedaldi, and A. Zisserman. The devil is in the details: an evaluation of recent feature encoding methods. In *Proc. BMVC.*, 2011. 4
- [5] K. Chatfield, K. Simonyan, A. Vedaldi, and A. Zisserman. Return of the devil in the details: Delving deep into convolutional nets. In *Proc. BMVC.*, 2014. 3
- [6] X. Chen and A. Yuille. Articulated pose estimation by a graphical model with image dependent pairwise relations. In *NIPS*, 2014. 1, 7
- [7] A. Cherian, J. Mairal, K. Alahari, and C. Schmid. Mixing body-part sequences for human pose estimation. In *CVPR*, 2014. 2, 3, 4, 5, 6, 7, 8
- [8] N. Dalal and B. Triggs. Histograms of oriented gradients for human detection. In *CVPR*, pages 886–893, 2005. 4
- [9] N. Dalal, B. Triggs, and C. Schmid. Human detection using oriented histograms of flow and appearance. In *ECCV*, pages 428–441, 2006. 4
- [10] J. Deng, W. Dong, R. Socher, L. jia Li, K. Li, and L. Fei-fei. Imagenet: A large-scale hierarchical image database. In *In CVPR*, 2009. 3
- [11] M. Douze and H. Jégou. The Yael library. In *ACM Multimedia*, 2014. 4
- [12] K. Duan, D. Parikh, D. Crandall, and K. Grauman. Discovering localized attributes for fine-grained recognition. In *CVPR*, pages 3474–3481, 2012. 1
- [13] G. Farnebäck. Two-frame motion estimation based on polynomial expansion. In *Proceedings of the 13th Scandinavian Conference on Image Analysis*, pages 363–370, 2003. 4
- [14] M. A. Fischler and R. C. Bolles. Random sample consensus: A paradigm for model fitting with applications to image analysis and automated cartography. *Commun. ACM*, pages 381–395, 1981. 4
- [15] R. Girshick, J. Donahue, T. Darrell, and J. Malik. Rich feature hierarchies for accurate object detection and semantic segmentation. In *CVPR*, pages 580–587, 2014. 2
- [16] G. Gkioxari and J. Malik. Finding action tubes. *arXiv 1411.6031*, 2014. 2, 3
- [17] H. Jhuang, J. Gall, S. Zuffi, C. Schmid, and M. J. Black. Towards understanding action recognition. In *ICCV*, pages 3192–3199, 2013. 1, 2, 3, 4, 5, 6, 7
- [18] A. Krizhevsky, I. Sutskever, and G. E. Hinton. ImageNet classification with deep convolutional neural networks. In *NIPS*. 2012. 1, 2
- [19] H. Kuehne, H. Jhuang, E. Garrote, T. Poggio, and T. Serre. HMDB: a large video database for human motion recognition. In *ICCV*, 2011. 1, 4
- [20] I. Laptev, M. Marszałek, C. Schmid, and B. Rozenfeld. Learning realistic human actions from movies. In *CVPR*, 2008. 1, 4
- [21] Y. LeCun, L. Bottou, Y. Bengio, and P. Haffner. Gradient-based learning applied to document recognition. *Proceedings of the IEEE*, pages 2278–2324, 1998. 1, 2
- [22] D. Oneata, J. Verbeek, and C. Schmid. Action and Event Recognition with Fisher Vectors on a Compact Feature Set. In *ICCV*, pages 1817–1824, 2013. 3, 4, 6

- [23] M. Oquab, L. Bottou, I. Laptev, and J. Sivic. Learning and transferring mid-level image representations using convolutional neural networks. In *CVPR*, pages 1717–1724, 2014. [2](#)
- [24] F. Perronnin, J. Sánchez, and T. Mensink. Improving the fisher kernel for large-scale image classification. In *ECCV*, pages 143–156. 2010. [2](#), [4](#)
- [25] L. Pishchulin, M. Andriluka, P. Gehler, and B. Schiele. Poselet conditioned pictorial structures. In *CVPR*, pages 588–595, 2013. [2](#)
- [26] M. Rohrbach, S. Amin, M. Andriluka, and B. Schiele. A Database for Fine Grained Activity Detection of Cooking Activities. In *CVPR*, 2012. [1](#), [4](#), [7](#)
- [27] B. Sapp and B. Taskar. Modec: Multimodal decomposable models for human pose estimation. In *CVPR*, 2013. [2](#), [3](#)
- [28] B. Sapp, D. Weiss, and B. Taskar. Parsing human motion with stretchable models. In *CVPR*, 2011. [2](#)
- [29] C. Schuldt, I. Laptev, and B. Caputo. Recognizing human actions: A local svm approach. In *Proc. ICPR*, pages 32–36, 2004. [1](#)
- [30] K. Simonyan and A. Zisserman. Two-stream convolutional networks for action recognition in videos. In *NIPS*, pages 568–576, 2014. [2](#)
- [31] K. Soomro, A. R. Zamir, and M. Shah. Ucf101: A dataset of 101 human actions classes from videos in the wild. In *CRCV-TR-12-01*, 2012. [3](#)
- [32] Y. Taigman, M. Yang, M. Ranzato, and L. Wolf. Deepface: Closing the gap to human-level performance in face verification. In *CVPR*, pages 1701–1708, 2014. [2](#)
- [33] J. J. Tompson, A. Jain, Y. LeCun, and C. Bregler. Joint training of a convolutional network and a graphical model for human pose estimation. In *NIPS*, pages 1799–1807, 2014. [1](#)
- [34] A. Toshev and C. Szegedy. Deeppose: Human pose estimation via deep neural networks. In *CVPR*, pages 1653–1660, 2014. [2](#)
- [35] H. Wang, A. Kläser, C. Schmid, and C.-L. Liu. In *CVPR*, pages 3169–3176, Colorado Springs, United States, 2011. [3](#)
- [36] H. Wang, A. Klser, C. Schmid, and C.-L. Liu. Dense trajectories and motion boundary descriptors for action recognition. *IJCV*, pages 60–79, 2013. [3](#)
- [37] H. Wang and C. Schmid. Action recognition with improved trajectories. In *ICCV*, 2013. [1](#), [2](#), [3](#), [4](#), [6](#)
- [38] Y. Yang and D. Ramanan. Articulated pose estimation with flexible mixtures-of-parts. In *CVPR*, pages 1385–1392, 2011. [1](#), [2](#), [3](#), [6](#)
- [39] N. J. Yue-Hei, H. Matthew, V. Sudheendra, V. Oriol, M. Rajat, and T. George. Beyond short snippets: Deep networks for video classification. In *CVPR*, 2015. [2](#)
- [40] Y. Zhou, B. Ni, S. Yan, P. Moulin, and Q. Tian. Pipelining localized semantic features for fine-grained action recognition. In *ECCV*, pages 481–496. 2014. [7](#)